SUPER-RAPID SCAN SATELLITE IMAGERY ANALYSIS OF TWO HAILSTORMS SAMPLED BY HAILSTONE

Jennifer M. Laflin* and Scott F. Blair
NOAA/NWS Kansas City/Pleasant Hill, Missouri

Chad Gravelle
NOAA/NWS Operations Proving Ground, CIMSS, University of Wisconsin–Madison

Kristopher Bedka
NASA Langley Research Center

Benjamin Scarino
Science Systems and Applications, Inc.

Jason Apke
University of Alabama-Huntsville

Cameron R. Homeyer
University of Oklahoma, Norman, Oklahoma

1. Introduction

Over the last several years, the Geostationary Operational Environmental Satellite (GOES)-14 Super Rapid Scan Operations for GOES-R (SRSOR) has occasionally operated in an experimental 1-minute mode to serve testbed and proving ground evaluations, as well as research efforts, leading up to the launch of GOES-R in November of 2016. These SRSOR periods were also coincident with operations of the field campaign A Hail Spatial and Temporal Observing Network Effort (HailSTONE) on two occasions: 10 May 2014 and 25 May 2015, both in northeast Kansas. The high spatiotemporal resolution of the hail observations collected by HailSTONE and the high temporal resolution of SRSOR provides a unique opportunity to compare satellite and hail observations on similar scales in severe convective weather environments. Products that were evaluated and compared to the reports collected by HailSTONE include infrared and visible satellite imagery, cloud-top divergence and absolute vorticity, lightning flash rate, and the radar-derived updraft character. Comparisons were then made in order to draw relationships between the SRSOR and lightning flash observations and the production of severe hail, and to help evaluate the utility of SRSOR imagery and derived products during severe convective warning operations.

Corresponding author address: Jennifer M. Laflin, NOAA/NWS Kansas City/Pleasant Hill, MO, 64080 email: jennifer.laflin@noaa.gov

2. Data and Methodology

a. HailSTONE Observations

Hail observations in this study were collected by A Hail Spatial and Temporal Observing Network Effort (HailSTONE; Blair et al. 2014, Blair et al., submitted), which was a field campaign aimed at capturing the true hail-fall of convective storms. Maximum and average hail diameter were observed in real-time for both cases, which mitigates much of the impact of melting on hail size at the time of measurement, and also provides a higher spatial and temporal resolution of hail reports than from traditional hail report sources like *Storm Data*. Since the spatiotemporal resolution of SRSOR data is much greater than the reports in *Storm Data*, it is important to compare the features and trends in these data with observations of similar resolution. In addition, *Storm Data* were found by Blair et. al (submitted) to significantly underrepresent the true maximum hail size produced in storms, which limits its ability to be useful for the calibration of satellite features, radar and lightning data, and other imagery and observations to specific hail size.

b. Radar, Satellite, and Lightning Data

Weather Surveillance Radar 1988-Doppler (WSR-88D) data were used in conjunction with HailSTONE reports to identify and attribute hail to specific convective storm cells. Volume scans from individual radar sites were first composited into a 4-D mosaic with 2 km spatial, 1 km vertical, and 5 min temporal resolution (Homeyer 2014, Homeyer and Kumjian 2015); then, radar cells were identified using local maxima of the echo tops (≥ 30 dBZ) exceeding the altitude of the environmental freezing level. Radar cells were linked to create tracks if they are within 15 km of each other in consecutive volume scans, and these tracks were retained if persistent for at least 15 min (3 volume scans; Homeyer et al., submitted). These data were then used to determine the periods of radar-derived updraft intensification, peak updraft, and updraft weakening for each storm cell attributed to HailSTONE reports.

GOES-14 SRSOR observations and derived products were then associated with each storm cell that was sampled by HailSTONE. Data recorded were the coldest infrared (IR) brightness temperatures (BT), overshooting tops (OT) detections in visible and IR (Bedka and Khlopenkov 2016), the difference in brightness temperature between OTs and the storm anvil (OT-Anvil BTD), and cloud-top divergence and absolute vorticity (Akpe et al. 2016). In addition, Earth Networks Total Lightning Network (ENTLN) lightning flash detections were accumulated at 1 min time-steps and within 8 km grid boxes, to best approximate the GOES-16 Global Lightning Mapper (GLM). Any flashes occurring within 15 km of radar cell center were attributed to that cell (Bedka et al. 2015) and used for analysis in this study.

3. Results

a. 25 May 2015

Several supercells developed on the afternoon of 25 May 2015 across northeast Kansas, in an environment characterized by 1500-2500 J kg^{-1} of mixed-layer convective available potential energy (MLCAPE), steep midlevel lapse rates, and 25-35 kts of 0-6 km bulk shear. The eastern-most supercell was sampled by HailSTONE between 2133–2210 UTC; however, since this event occurred outside the main field operations period, real-time in-situ observations were limited by a low availability of intercept vehicles. In total, 9 measured hail reports were collected for this cell over the 37 min period, ranging in diameter from 1.00 in. to 4.75 in. Hail sizes steadily increased from 2133 to 2142 UTC, when the maximum diameter hail of 4.75 in. was recorded.

From a radar perspective, the cell reached its peak strength just prior to the observation of large hail. At 2123 UTC, a bounded weak echo region (BWER) was evident in reflectivity at 20,000 ft on the KTLX Topeka, KS WSR-88D, indicative of a strong thunderstorm updraft (Fig. 1). In addition, the maximum rotational velocity (V_r) at 20,000 ft on the 2123 UTC KTLX radar volume scan was 58 kts, within a V_r range associated with the production of giant hail (diameter ≥ 4.00 in.; Blair et al. 2011). Once increasing hail size was observed at the surface by HailSTONE, the cell was beginning to weaken and become a bit more disorganized as it lost its defined BWER in reflectivity and large V_r in velocity, both at approximately 20,000 ft (2134 UTC; Fig. 2).

SRSOR imagery shows a similar trend in storm behavior as it relates to the observation of hail. OTs are evident in both visible and IR imagery between 2116 and 2141 UTC, and appear most defined while coincident with a lightning flash rate greater than 20 flashes per minute between 2118 and 2121 UTC (Fig. 3). OT brightness temperatures were also at their coldest and the BT-difference was greatest during the updraft intensification phase just prior to 2120 UTC, which was maintained through the initial observation of hail at 2133 UTC (Fig. 4). Maximum cloud-top divergence and absolute vorticity both fell slightly during the period of updraft intensification, but then increased again just when hail was beginning to be observed at the surface, and decreasing again there-after (Fig. 5). In general, SRSOR imagery and satellite derived products showed the cell at peak strength just prior to observed hail, and large hail reached the ground as the updraft weakened.

b. 10 May 2014

While 10 May 2014 is best known for the robust supercells that occurred in Missouri, including the cell which produced an EF-2 tornado in Orrick; a few supercells also formed earlier that afternoon just west of the Missouri/Kansas border. The combination of a triple-point dryline/warm front intersection in northeast Kansas, along with 1500-2500 J kg^{-1} of MLCAPE and greater than 50 kts of 0-6 km bulk shear, was enough to both support the initiation and supercell mode of storms which developed in that area. HailSTONE was again operating with limited vehicle availability but collected 14 hail reports, ranging in diameter from 0.25 to 2.00 in., over the 47 min period that spanned 2152–2239 UTC.

Supercell characteristics were identifiable in KTLX WSR-88D data both prior to and during the observation of large hail by HailSTONE. At 2147 UTC (Fig. 6; 9 min prior to the first occurrence of 1.00 in. hail, and 23 min prior to the 2.00 in. hail observation), V_r was 36 kts at approximately 20,000 ft, which falls in the median range for 1.75-2.00 in. hail (Blair et. al 2011). During large hail fall and just prior to the 2.00 in. hail report (2205 UTC; Fig. 7), V_r had decreased but modest midlevel rotation and a persistent three-body scatter spike (TBSS) were still evident at the approximate 20,000 ft level. A subtle, transient BWER was also evident ten min prior to the 2.00 in. hail report, but was no longer apparent by the 2205 UTC volume scan.

In contrast to radar analysis, satellite imagery and products were much less impressive for this cell. Visible and IR OT detections did not occur during this storm's life cycle, and minimum BTs hovered right around 220 K throughout. In the imagery, the storm updraft appeared strongly sheared off to the east in visible, and especially IR (Fig. 8), which may have contributed to the lack of identifiable supercellular features in SRSOR, and is seemingly consistent with the higher environmental deep-layer shear. Two strengthening, peak intensity, and weakening phases were observed with this cell, between 2140–2155 UTC and between 2159–2216 UTC; both which were characterized by increasing cloud-top divergence and absolute vorticity during the peak intensity phase, and then decreases in both of these derived products during the updraft weakening phase (Fig 9). Lightning flash rate was also fairly low throughout the life cycle of the cell, but jumped twice to a value greater than 20 flashes per minute over an 8 km grid box between 2145–2148 UTC — the same time period that the maximum V_r was also observed in radar data.

4. Discussion and Summary

Two supercell cases are presented in this study, and the unique combination of both high-resolution SRSOR and HailSTONE data allows the comparison of observations on similar spatiotemporal scales. Even during limited HailSTONE operations which produced a lower number of total hail reports than typically observed during the primary operating period of the field campaign, the resolution still far exceeds that found in *Storm Data* and better captures the true maximum hail diameter produced by these storms — in the 25 May 2015 case, the maximum hail size observed by HailSTONE exceeded the maximum diameter recorded in *Storm Data* by 2.25 in.

Despite many similarities in the environment, geographic location, time of year and time of day, and storm mode, these two cases exhibited quite different behavior prior to and during observed hail fall. The 25 May 2015 case was a bit more prototypical, showing many of the same supercell characteristics identified by Blair et al. (2011) and Bedka et al. (2015), and showing signs of peak updraft intensity and supercell organization aloft prior to the observation of large hail at the surface. While the 10 May 2014 storm could be defined as a supercell in radar data and fit well within the expected rotational velocity for 1.75-2.00 in. hail-producing supercells, SRSOR data were muddier and provided little additional information about the storm strength or character. In addition, observed large hail fall occurred during peak updraft intensity versus the updraft weakening phase, which could be related to the multiple pulses in updraft strength; one which occurred several minutes prior to the observation of large hail at the surface.

In both cases, the rapid pace of changes in storm behavior, organization, and intensity observed in radar, lightning, and SRSOR underscores the importance of comparing data of similar resolution. In addition, the difference in the sizes and general availability of *Storm Data*, particularly for the 25 May 2015 case, provides an example of why caution should be used when relating specific features in observational data or creating "rules of thumb" for particular hail sizes when the true hail fall may not be known. In order to better correlate and use GOES-16 imagery and derived products along with WSR-88D data, it is important to expand this research to many more storms of varying intensity. One opportunity to better understand these correlations would be during the GOES-R Field Campaign, which will is tentatively scheduled for the spring of 2017.

5. References

Apke, J. M., J. R. Mecikalski, and C. P. Jewett, 2016: Analysis of mesoscale atmospheric flows above mature deep convection using super rapid scan geostationary satellite data. J. *Appl. Meteor. Climatol.*, **55**, 1859-1887.

Bedka, K. M., C. Wang, R. Rogers, L. Carey, W. Feltz, and J. Kanak, 2015: Examining deep convective cloud evolution using total lightning, WSR-88D, and GOES-14 super rapid scan datasets. *Wea. Forecasting*, **30**, 571–590.

Bedka, K. M., and K. Khlopenkov, 2016: A probabilistic multispectral pattern recognition method for detection of overshooting cloud tops using passive satellite imager observations. *J. Appl. Meteor. Climatol*., **55**, 1983-2005.

Blair, S. F., D. R. Deroche, J. M. Boustead, J. W. Leighton, B. L. Barjenbruch, and W. P. Gargan, 2011: A radar-based assessment of the detectability of giant hail. *Electronic J. Severe Storms Meteor.*, **6** (7), 1–30.

Blair, S. F., D. E. Cavanaugh, J. M. Laflin, J. W. Leighton, K. J. Sanders, and K. L. Ortega, 2014: High-resolution hail observations: Implications for NWS warning operations and climatological data. *27th Conf. on Severe Local Storms*, Madison, WI, Amer. Meteor. Soc., AMS Online, 18.1.

Blair, S. F., and coauthors: High-resolution hail observations: Implications for NWS warning operations. *Wea. Forecasting*, submitted.

Homeyer, C. R., 2014: Formation of the enhanced-V infrared cloud-top feature from high-resolution three-dimensional radar observations. *J. Atmos. Sci.*, **71**, 332-348.

Homeyer, C. R., and M. R. Kumjian, 2015: Microphysical characteristics of overshooting convection from polarimetric radar observations. *J. Atmos. Sci.*, **72**, 870-891.

Homeyer, C. R., J. D. McAuliffe, and K. M. Bedka: On the development of above-anvil cirrus plumes in extratropical convection. *J. Atmos. Sci.*, submitted.

6. Figures

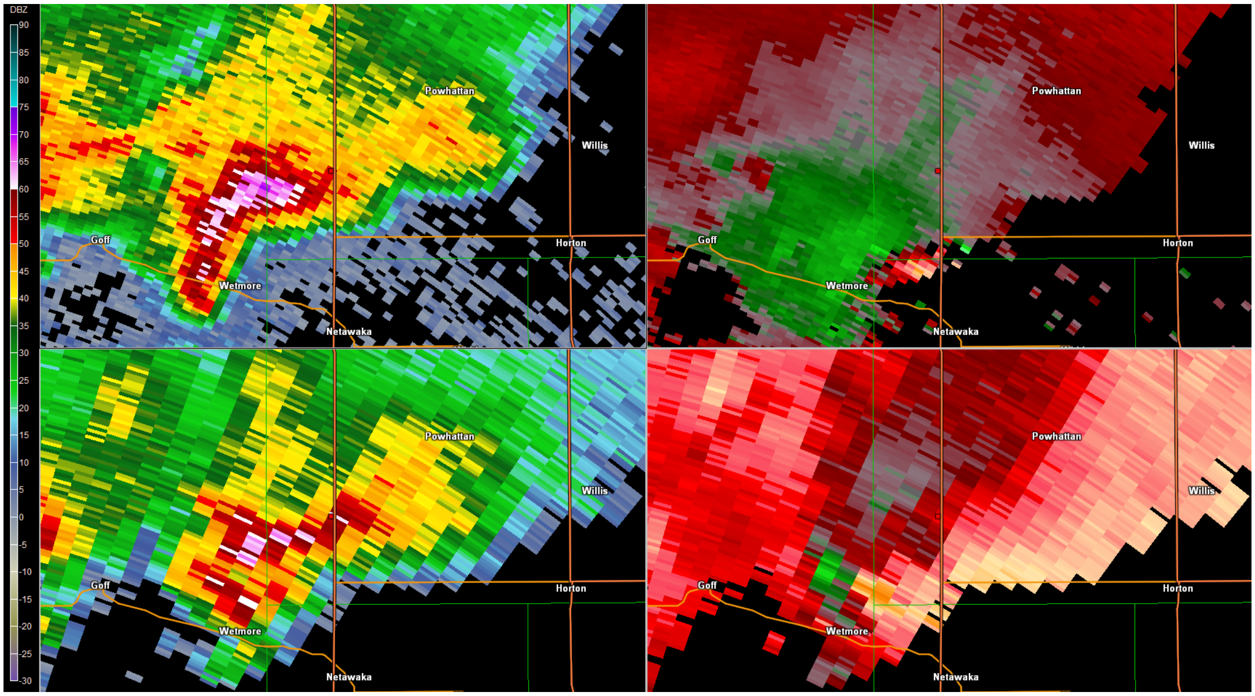

Figure 1. 4-panel of KTWX WSR-88D radar data at 2123 UTC on 25 May 2015. Clockwise, from the upper left: 0.5° reflectivity, 0.5° storm-relative velocity, 4.1° reflectivity, and 4.1° storm-relative velocity.

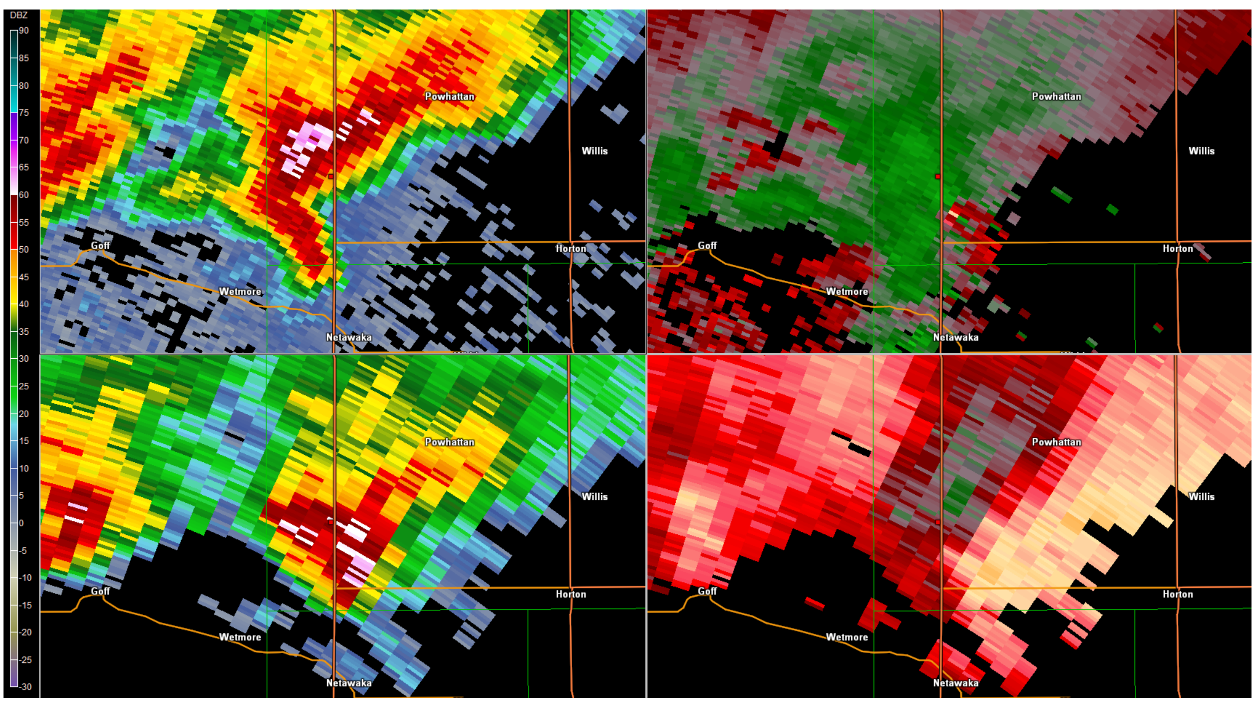

Figure 2. 4-panel of KTWX WSR-88D radar data at 2134 UTC on 25 May 2015. Clockwise, from the upper left: 0.5° reflectivity, 0.5° storm-relative velocity, 4.1° reflectivity, and 4.1° storm-relative velocity.

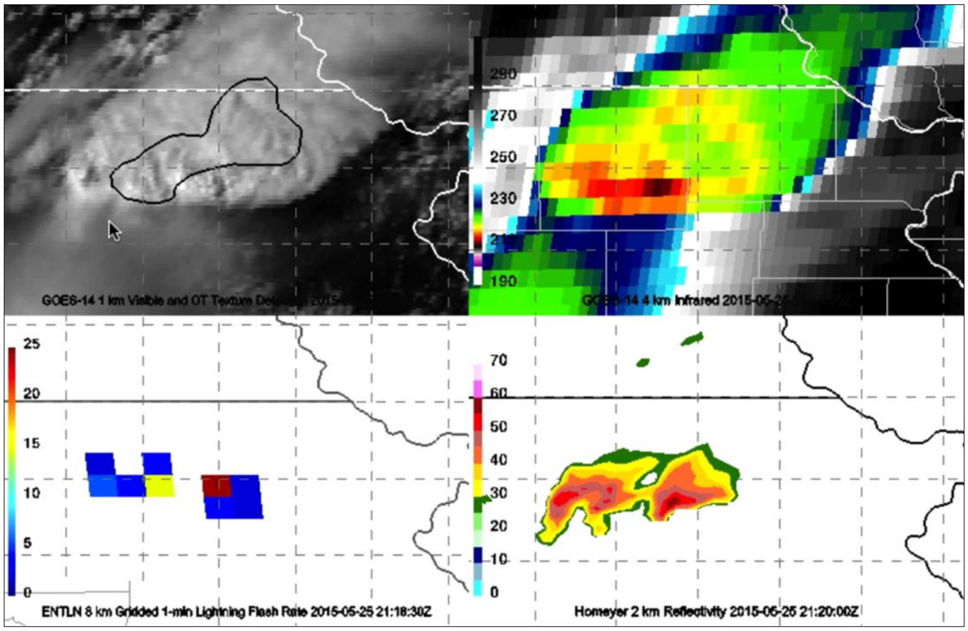

Figure 3. 4-panel of GOES-14 SRSOR imagery, ETLTN data, and radar reflectivity at 2119 UTC on 25 May 2015. Clockwise, from the upper left: 1 km visible satellite imagery, 4 km infrared satellite imagery, 2 km gridded base reflectivity, and ENTLN 8-km gridded lightning flash rate.

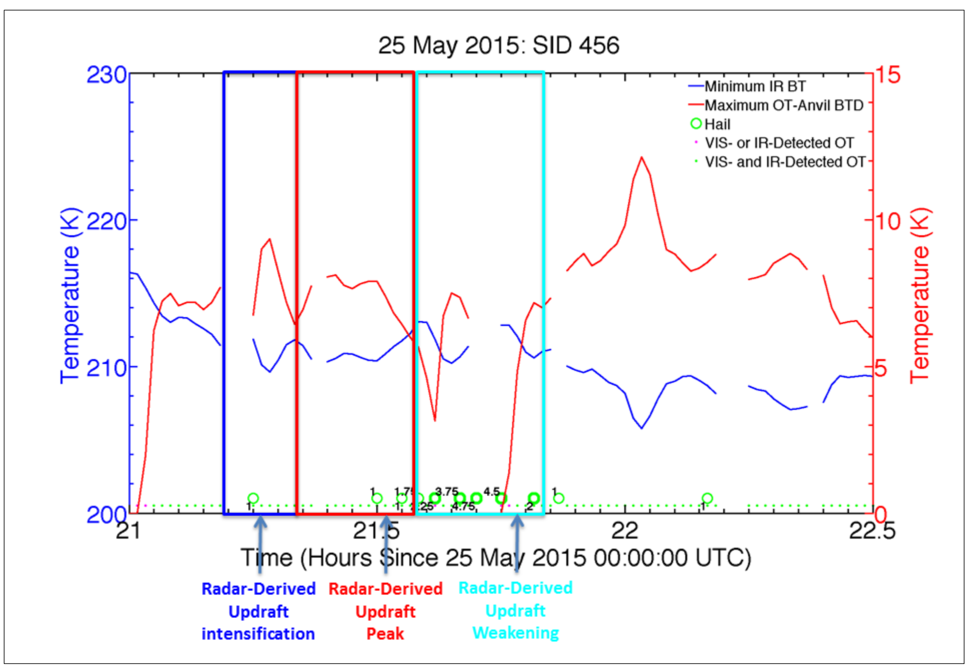

Figure 4. SRSOR-derived minimum infrared brightness temperature (blue line), maximum difference in brightness temperature (K) between overshooting tops and thunderstorm anvil (red line), HailSTONE hail reports (green open circles), overshooting top detections in both visible and infrared satellite (green dots), and overshooting top detections in either visible or infrared satellite (pink dots) for the 25 May 2015 case. Data are binned by periods of radar-derived updraft intensification (blue outlined box), updraft peak (red outlined box), and updraft weakening (cyan outlined box).

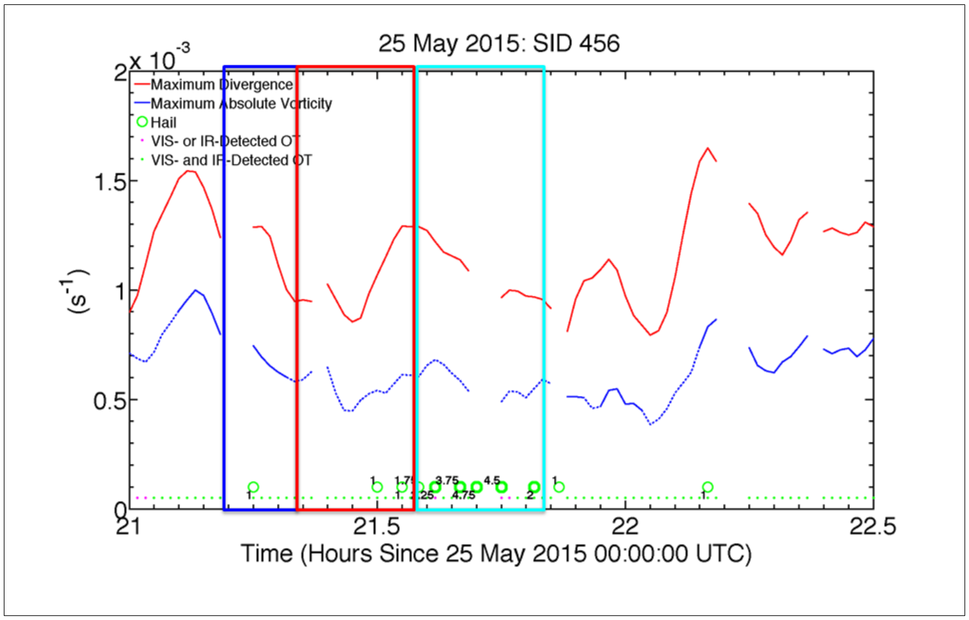

Figure 5. SRSOR-derived maximum cloud top divergence (red line), maximum absolute vorticity (blue line), HailSTONE hail reports (green open circles), overshooting top detections in both visible and infrared satellite (green dots), and overshooting top detections in either visible or infrared satellite (pink dots) for the 25 May 2015 case. Data are binned by periods of radar-derived updraft intensification (blue outlined box), updraft peak (red outlined box), and updraft weakening (cyan outlined box).

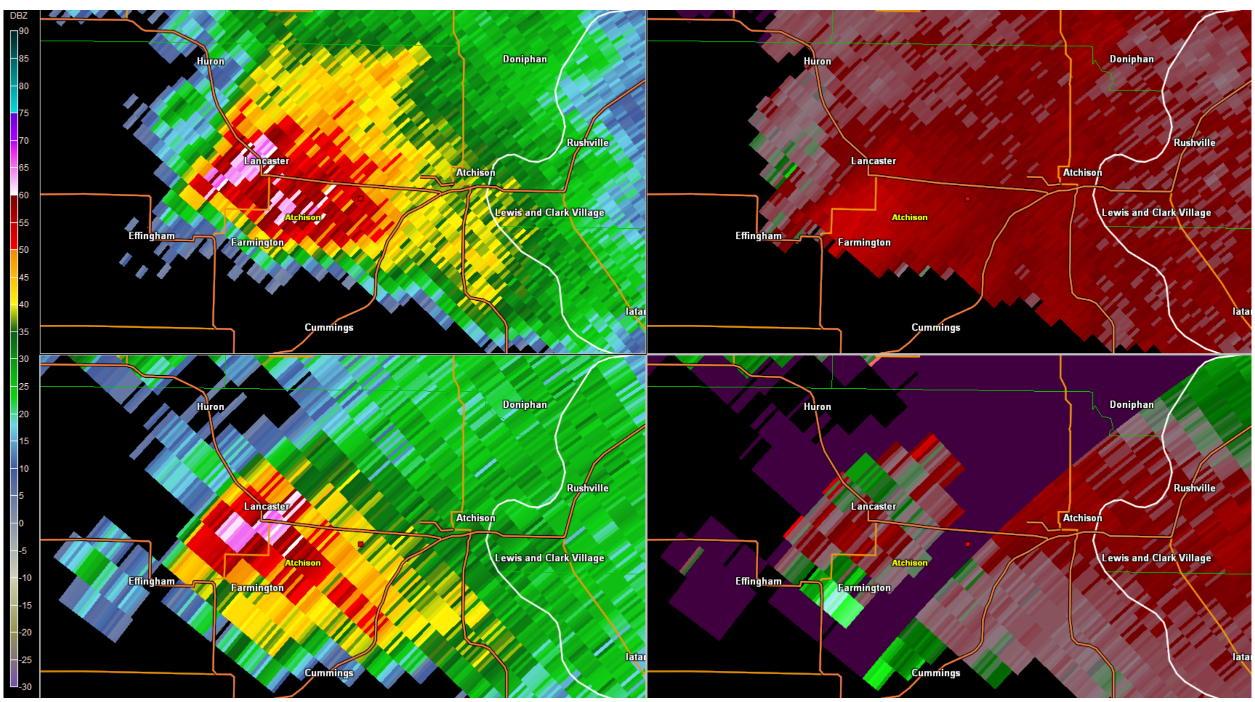

Figure 6. 4-panel of KEAX WSR-88D radar data at 2147 UTC on 10 May 2014. Clockwise, from the upper left: 0.5° reflectivity, 0.5° storm-relative velocity, 4.1° reflectivity, and 4.1° storm-relative velocity.

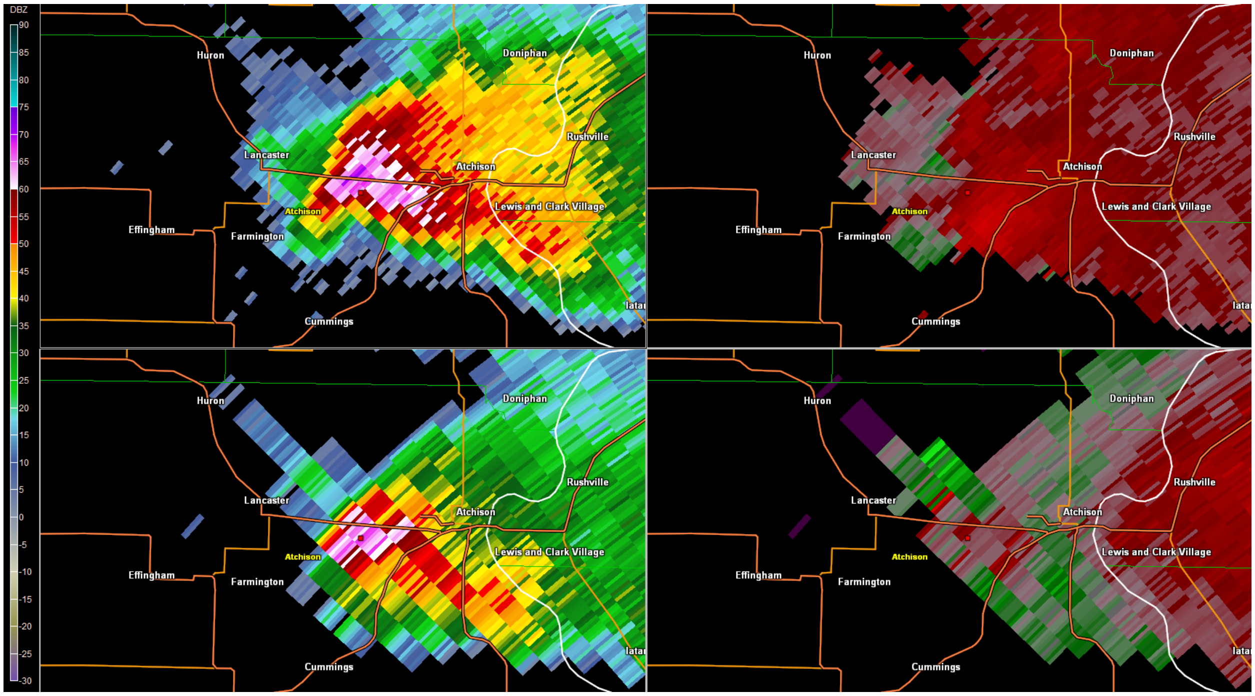

Figure 7. 4-panel of KEAX WSR-88D radar data at 2205 UTC on 10 May 2014. Clockwise, from the upper left: 0.5° reflectivity, 0.5° storm-relative velocity, 4.1° reflectivity, and 4.1° storm-relative velocity.

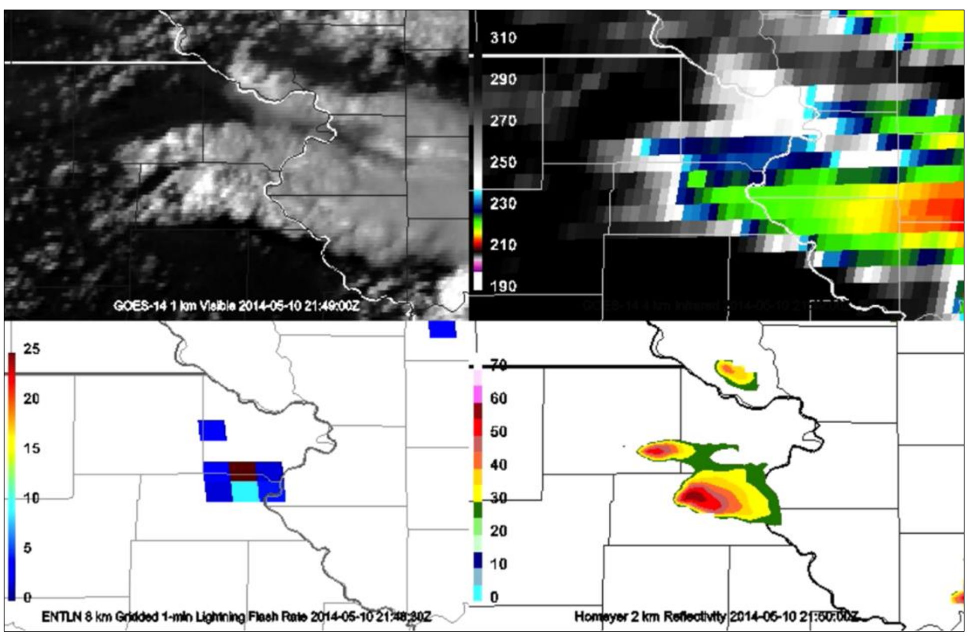

Figure 8. 4-panel of GOES-14 SRSOR imagery, ETLTN data, and radar reflectivity at 2149 UTC on 10 May 2014. Clockwise, from the upper left: 1 km visible satellite imagery, 4 km infrared satellite imagery, 2 km gridded base reflectivity, and ENTLN 8-km gridded lightning flash rate.

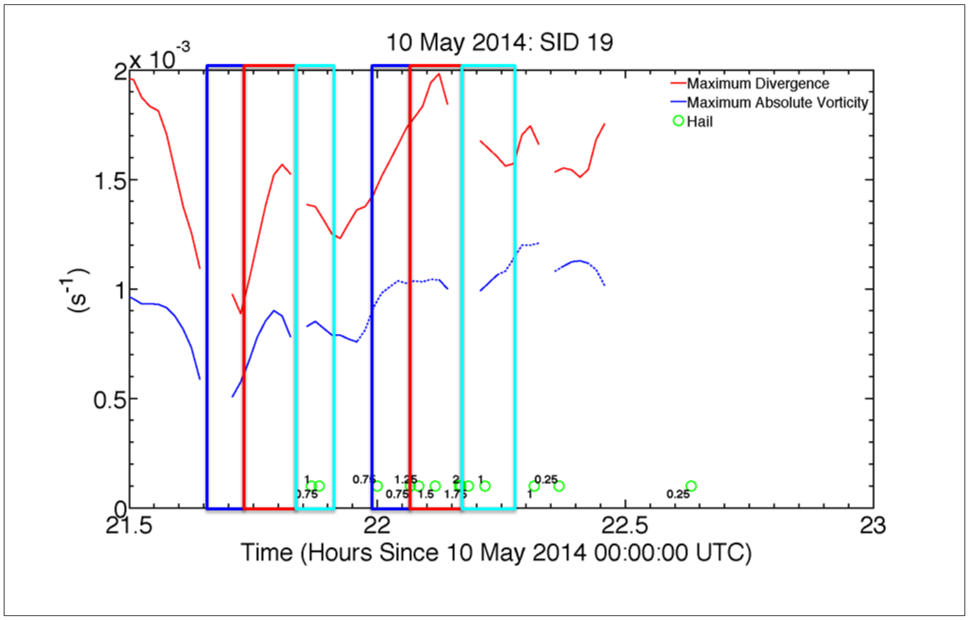

Figure 9. SRSOR-derived maximum cloud top divergence (red line), maximum absolute vorticity (blue line), HailSTONE hail reports (green open circles), overshooting top detections in both visible and infrared satellite (green dots), and overshooting top detections in either visible or infrared satellite (pink dots) for the 10 May 2014 case. Data are binned by periods of radar-derived updraft intensification (blue outlined box), updraft peak (red outlined box), and updraft weakening (cyan outlined box).